

Rawsamble: Overlapping and Assembling Raw Nanopore Signals using a Hash-based Seeding Mechanism

Can Firtina¹ Maximilian Mordig^{1,2} Harun Mustafa^{1,3,4} Sayan Goswami¹ Nika Mansouri Ghiasi¹
Stefano Mercogliano¹ Furkan Eris¹ Joël Lindegger¹ Andre Kahles^{1,3,4} Onur Mutlu¹
¹ETH Zurich ²Max Planck Institute for Intelligent Systems
³University Hospital Zurich ⁴Swiss Institute of Bioinformatics

Abstract: Raw nanopore signal analysis is a common approach in genomics to provide fast and resource-efficient analysis without translating the signals to bases (i.e., without basecalling). However, existing solutions cannot interpret raw signals directly if a reference genome is unknown due to a lack of accurate mechanisms to handle increased noise in pairwise raw signal comparison. Our goal is to enable the direct analysis of raw signals without a reference genome. To this end, we propose Rawsamble, the first mechanism that can 1) identify regions of similarity between all raw signal pairs, known as all-vs-all overlapping, using a hash-based search mechanism and 2) use these to construct genomes from scratch, called *de novo* assembly.

Our extensive evaluations across multiple genomes of varying sizes show that Rawsamble provides a significant speedup (on average by 16.36× and up to 41.59×) and reduces peak memory usage (on average by 11.73× and up to 41.99×) compared to a conventional genome assembly pipeline using the state-of-the-art tools for basecalling (Dorado’s fastest mode) and overlapping (minimap2) on a CPU. We find that 36.57% of overlapping pairs generated by Rawsamble are identical to those generated by minimap2. Using the overlaps from Rawsamble, we construct the first *de novo* assemblies directly from raw signals without basecalling. We show that we can construct contiguous assembly segments (unitigs) up to 2.7 million bases in length (half the genome length of *E. coli*). We identify previously unexplored directions that can be enabled by finding overlaps and constructing *de novo* assemblies.

Availability and Implementation: Rawsamble is available at <https://github.com/CMU-SAFARI/RawHash>. We also provide the scripts to fully reproduce our results on our GitHub page.

1. Introduction

Nanopore sequencing technology [1–23] can sequence long nucleic acid molecules of up to a few million bases at high throughput [24–26]. As a molecule moves through a tiny pore, called a *nanopore*, ionic current measurements, called *raw signals*, are generated [5]. Nanopore

sequencing provides three unique key benefits.

First, nanopore sequencing enables stopping the sequencing of single reads or the entire sequencing run early, known as *adaptive sampling* or *selective sequencing* [27], while raw signals are generated and analyzed during sequencing, called *real-time analysis*. Adaptive sampling can substantially reduce the sequencing time and cost by avoiding unnecessary sequencing. Second, raw nanopore signals retain more information than nucleotides, such as methylation, and can be useful for many applications [28]. Third, compact nanopore sequencing devices enable on-site portable sequencing and analysis, which can be coupled with real-time analysis [29].

Existing works that analyze raw nanopore signals [27, 30–66] mainly utilize deep learning mechanisms [30–47] to translate these signals into nucleotides, a process called *basecalling*. Basecalling mechanisms usually 1) are designed to use large chunks of raw signal data for accurate analysis [53] and 2) have high computational requirements [26, 60]. This can impose limitations to enable 1) accurate real-time analysis [53] and 2) portable sequencing with constrained resources [60].

To fully utilize the unique benefits of nanopore sequencing, it is necessary to analyze raw signals with 1) high accuracy and low latency for adaptive sampling and 2) low resource usage for portability and efficiency. To achieve this, several mechanisms focus on analyzing raw nanopore signals *without* basecalling [27, 52–66].¹ Although raw nanopore signal mapping to a reference genome is widely studied to achieve relatively accurate and fast mapping of raw signals [27, 53, 54, 57–60, 62–66], none of these works *without* a reference genome.

When a reference genome is not available, a genome can be constructed from scratch, called *de novo* assembly construction [67]. To construct a *de novo* assembly, similar regions between all read pairs are identified, called *all-vs-all overlapping*, instead of identifying similarities between reads and a reference genome. [26, 68, 69]. How-

¹We use the *raw signal analysis* term specifically for these mechanisms in the remainder of the paper.

ever, an all-vs-all overlapping between raw nanopore signals remains unsolved due to several unique challenges [5, 70–72].

First, it is challenging to identify similarities between a pair of noisy raw signals as compared to a noisy raw signal and an accurate signal generated from a reference genome, an approach commonly used in earlier works for read mapping [53, 54, 57–59]. This is because converting reference genomes to their expected raw signal values is free from certain types of noise that raw nanopore signals contain (e.g., stochastic signal fluctuations [5] and variable speed of DNA molecules moving through nanopores [70, 71]), while none of the raw signals are free from such noise in all-vs-all overlapping.

Second, existing raw signal analysis works lack the mapping strategies typically used in all-vs-all overlapping, such as reporting multiple mappings (i.e., overlaps) of a read to many reads. This is because these works are mainly designed to stop the mapping process as soon as there is an accurate mapping for a read to minimize the unnecessary sequencing [54]. For all-vs-all overlapping, pairwise mappings of a read to many reads (instead of a single mapping) must be reported while avoiding certain trivial cyclic pairwise mappings to construct an assembly [68].

Third, read overlapping can increase the space requirements for storing and using indexing. This is because a read set is likely to be sequenced such that its overall number of bases is larger than the number of bases in its corresponding genome. Such an increased index size can raise the computational and space demands for read overlapping. It is essential to provide high-throughput and scalable computation to enable real-time downstream analysis for future work (as discussed in Section 4).

Our goal is to enable 1) raw signal analysis *without* a reference genome and 2) new use cases with raw nanopore signal analysis, such as *assembly from overlapping* raw signals, by addressing the challenges of accurate and fast all-vs-all overlapping of raw nanopore signals. To this end, we propose *Rawsamble*, the first mechanism that enables fast and accurate overlap finding between raw nanopore signals. The key idea in *Rawsamble* is to re-design the existing state-of-the-art hash-based seeding mechanism [58, 59] for raw signals with more effective noise reduction techniques and useful outputting strategies to find all overlapping pairs accurately, which we explain in three key steps.

First, to enable identifying similarities between a pair of noisy raw signals accurately, *Rawsamble* filters raw

signals to select those substantially distinct from their surrounding signals. Such non-distinct and adjacent signals are usually the result of a certain error type in the analysis, known as *stay errors* [53, 58, 63]. Although similar filtering strategies [53, 58, 63] are exploited when mapping raw signals to reference genomes, *Rawsamble* performs a more aggressive filtering to avoid storing the erroneous portions of signals in the index to enable accurate similarity identification from the sufficiently distinct regions of signals. Second, to find multiple overlaps for a read, *Rawsamble* identifies highly accurate chains from seed matches based on their chaining scores and reports *all* of these chains as mappings, as opposed to choosing solely the best mapping as determined by weighted decisions among all such chains [59]. Third, to prevent trivial cycles between a pair of overlapping reads, *Rawsamble* ensures that only one of the overlapping reads in each pair is always chosen as a query sequence, and the other is always chosen as a target sequence based on a deterministic ordering mechanism between these reads. These steps enable *Rawsamble* to find overlaps between raw signals accurately and quickly.

Rawsamble makes the following key contributions:

- We propose the *first* mechanism that can find all-vs-all overlapping of raw signals without basecalling to enable new use cases for raw signal analysis, such as assembling raw signals.
- We show that identifying overlaps with *Rawsamble* 1) is faster (on average $16.36\times$ and up to $41.59\times$) and 2) reduces peak memory requirements (on average $11.73\times$ and up to $41.99\times$) compared to the computational pipeline that includes the state-of-the-art basecalling running on a CPU with its fastest model followed by *minimap2* to find overlaps. We evaluate the trade-offs between speed, accuracy, and hardware resources by running the basecaller on a CPU and GPU with fast and high-accuracy models.
- We show that 36.57% of overlapping pairs that *Rawsamble* generates are identical to the overlapping pairs generated by *minimap2*.
- We report the first *de novo* assemblies ever constructed directly from raw signal overlaps without basecalling. We show that we can construct long unitigs up to 2.7 million bases in length for *E. coli*, which constitutes half the length of the genome.
- We discuss new use cases that can be enabled with overlapping raw signals and constructing assemblies from raw signals, such as new directions for improving the accuracy and performance of basecalling.

2. Methods

2.1. Overview

Rawsamble is a mechanism to find overlapping pairs between raw nanopore signals (i.e., *all-vs-all overlapping*) for constructing *de novo* assemblies without basecalling, as shown in Figure 1. To achieve this, Rawsamble builds on the state-of-the-art raw signal mapper, RawHash2 [58, 59]. We provide the overview of RawHash2 in Supplementary Section A. Rawsamble extends RawHash2 to support all-vs-all raw signal overlapping in four key steps: First, to enable efficient and accurate indexing from the noisy raw signals (1), Rawsamble aggressively filters the raw input after the signal-to-event conversion to avoid nanopore-related errors. Second, to improve the accuracy of overlapping (2), Rawsamble adjusts the minimum chaining score to avoid false chains, ensuring that only high-confidence overlaps are considered. Third, to enable finding useful and long connections from many overlaps, Rawsamble adjusts the output strategy such that 1) *all* chains rather than only the best chain are reported and 2) cyclic overlaps are avoided. Fourth, we introduce a new assembler to output the assembled sequences after performing *de novo* assembly from raw signal overlaps (3). Rawsamble enables the use of existing *de novo* assemblers such as miniasm [68] as it provides the overlap information in a standardized format that these assemblers use.

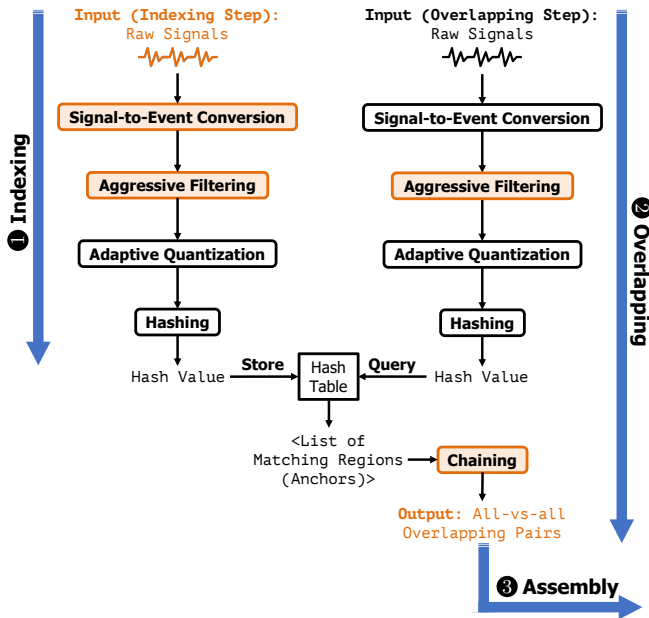


Figure 1: Overview of Rawsamble. We use colors for the inputs, steps, and outputs to highlight the parts that Rawsamble modifies over RawHash2.

2.2. Constructing an Index from Noisy Raw Signals via Aggressive Filtering

Rawsamble identifies overlapping regions between raw nanopore signals using a hash-based seeding mechanism that operates in two steps. First, to enable quick matching between raw signals, Rawsamble enables constructing an index directly from raw nanopore signals instead of using an existing reference genome sequence. While converting reference genomes to their expected raw signal values to store them in an index is mainly free from certain types of noise that raw nanopore signals contain (e.g., stochastic signal fluctuations [5] and variable speed of DNA molecules moving through nanopores [70, 71]), noise in raw nanopore signals can cause challenges to find accurate matches between raw signals when these signals are stored in an index. Second, to reduce noise stored in the hash tables and enable accurate similarity identification when both signals are noisy, Rawsamble aggressively filters raw signals as shown in Figure 2. The filtering mechanism iteratively compares two adjacent signals, s_i and s_j , and removes the second signal, s_j , if the absolute difference between the two adjacent signals is below a certain threshold T . This filtering generates a list of filtered signals that aggressively aims to reduce the impact of stay errors during sequencing. Although similar filtering approaches are used in prior works [53, 58, 59] to reduce the stay errors (e.g., by aiming to perform homopolymer compression of raw signals [63]), Rawsamble employs a substantially larger threshold (i.e., aggressive) for filtering to minimize noise both in the index and during mapping. By applying the aggressive filtering technique, Rawsamble ensures that only high-quality, informative events are used in indexing to improve the accuracy and efficiency of the overall overlapping mechanism when both signals are noisy.

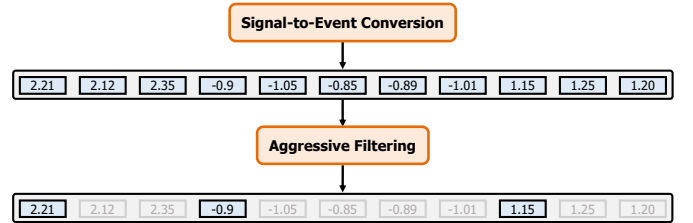


Figure 2: Filtering in Rawsamble. Values in gray boxes show the filtered signals as their values are close to the previous signal (in a blue box) that is not filtered out.

2.3. Adjusting the Chaining Mechanism for Overlapping

To reduce the number of chains that do not result in mapping (i.e., false chains) and construct longer chains,

Rawsamble adjusts the chaining mechanism [59, 73] in two ways. First, Rawsamble constructs chains between seed matches (i.e., anchors) with longer gaps by adjusting the maximum gap length between anchors. This adjustment is needed because the filtering mechanism results in a sparser list with potentially long gaps between signals. Second, to ensure that only high-confidence chains are considered as overlaps among many pairwise overlapping regions, Rawsamble sets a higher minimum chaining score for overlapping than mapping, which effectively filters out spurious matches. These adjustments to the chaining mechanism enable Rawsamble to construct long and accurate chains between noisy and sparse raw signals, improving the overall sensitivity of the overlapping process and further downstream analysis such as *de novo* assembly construction.

2.4. Adjusting the Mapping Strategy

Rawsamble adjusts the mapping strategy used in RawHash2 in two ways. First, Rawsamble generates pairwise mappings of a read to many reads (instead of a single mapping per read). To achieve this, Rawsamble identifies all valid chains based on their chaining scores and reports all such chains between raw signals. This enables overlapping a single raw signal with multiple other raw signals. Second, Rawsamble filters out *trivial* cyclic overlaps between two reads. To do so, Rawsamble avoids reporting overlapping signal pairs both as *query* and *target* in the mapping output, which can complicate the *de novo* assembly construction process [68, 74, 75]. To avoid these trivial cyclic overlaps, Rawsamble uses a pre-defined and deterministic ordering between raw signals (e.g., based on the lexicographic ordering of read names). By comparing raw signals deterministically, Rawsamble guarantees that only one of each pair of overlapping reads is processed as a query sequence while the other is treated as a target sequence. Reporting all chains while avoiding cyclic overlaps between raw signals allows for a comprehensive representation of the overlapping regions, which is useful for constructing accurate and long assemblies.

2.5. Signal Assembly from Overlaps

Rawsamble provides the overlapping information between raw signals using the Pairwise mApping Format (PAF) [68], which can be used by existing assemblers like miniasm [68] to construct an assembly as an assembly graph for output in Graphical Fragment Assembly (GFA) [68, 76] format.

To output the sequence of assembled signals directly from identified overlaps along with the assembly graph

in GFA format, Rawsamble provides a new assembler, Rawasm [77]. This assembler can be useful for facilitating complete *de novo* assembly without requiring basecalling or to aid the basecalling process in several ways, as we discuss in Section 4.

Rawasm is implemented as a small extension to miniasm, introducing three key modifications to enable outputting the assembled signals. First, to read raw signals and store the assembled signals in standard raw signal file formats, Rawasm supports all major raw signal file formats: FAST5, POD5, S/BLOW5 [78]. Second, to improve memory efficiency and reduce the significant I/O burden associated with reading and writing raw signal files, which are typically larger and stored in complex compressed formats compared to basecalled sequences, Rawasm implements several optimizations. Unlike miniasm, which keeps all unitigs in main memory until the GFA file is written, Rawasm overlaps the graph building and writing processes. When the signals for a unitig are trimmed for outputting, and their positions within the unitig are calculated, Rawasm updates the output and frees up the corresponding memory. This approach minimizes memory usage and I/O delays to improve efficiency and reduce I/O overhead. Third, to output the assembled signals without losing the additional important metadata associated with raw signals, Rawasm generates a new raw signal file for each unitig in the assembly graph by concatenating the original signals that construct the corresponding unitig. The concatenation mechanism trims and arranges the signals based on the start and end positions used for constructing the unitig as provided by the assembly graph, similar to miniasm. Since each raw signal may contain different metadata (e.g., signal variables determined based on the characteristics of a nanopore channel), Rawasm keeps this metadata associated with each raw signal.

The overlapping information that Rawsamble generates can be used by any assembler that takes Pairwise mApping Format (PAF) [68] as input, including Rawasm and miniasm [68]. Although any such assembler can construct assemblies from PAF and output the resulting assembly information in GFA, Rawasm is the first implementation to enable outputting the resulting assembly signals directly after from the resulting GFA.

3. Results

3.1. Evaluation Methodology

We implement the improvements we propose in Rawsamble on the RawHash2 implementation [59]. Similar to

RawHash2 and minimap2 [73], Rawsambl provides the mapping information in the standard Pairwise mApping Format (PAF) [68]. We basecall the signals on two different hardware setups using Dorado’s 1) high accuracy (HAC) and super high accuracy (SUP) models with an NVIDIA RTX A6000 GPU [79], and 2) fast (Fast) and high accuracy (HAC) models with an Intel Xeon Gold 6226R CPU [80]. We use Dorado’s 1) Fast model on a CPU to show the best performance (i.e., speed) that a CPU-based basecalling can provide and 2) SUP model on a GPU to show the best accuracy that basecalling provides along with its associated increased computational cost. We use POD5 files for all datasets, as suggested by Dorado [35] for optimal performance. Since no prior works can overlap reads using raw signals, we compare Rawsambl to minimap2, the current state-of-the-art read overlapper for basecalled sequences using the datasets shown in Table 1. We use datasets both with high sequencing depth of coverage (D1 to D3) and low coverage (D4 and D5) to evaluate the capability to construct assemblies in both scenarios.

Table 1: Details of datasets used in our evaluation.

	Organism	Device Type	Reads (#)	Bases (#)	Estimated Coverage (×)	SRA Accession
D1	SARS-CoV-2	MinION	10,001	4.02M	135×	CADDE Centre
D2	<i>E. coli</i>	GridION	353,948	2,332M	445×	ERR9127551
D3	<i>Yeast</i>	MinION	50,023	385M	32×	SRR8648503
D4	<i>Green Algae</i>	PromethION	30,012	622M	5.6×	ERR3237140
D5	<i>Human</i>	MinION	270,006	1,773M	0.6×	FAB42260

Base counts in millions (M). Coverage is estimated using corresponding reference genomes.

All datasets are generated using ONT’s R9.4.1 e8 flow cells (450 bp/sec translocation speed with 4000 signals/sec sampling frequency).

All of the datasets are basecalled using Dorado (HAC) v3.3.

We evaluate computational requirements in terms of overall run time with 32 CPU threads and peak memory usage. We use 32 CPU threads since the average thread utilization of CPU-based basecalling is around 32. We report the elapsed time, CPU time (when using only CPUs without GPUs), and peak memory usage of 1) minimap2 with and without basecalling and 2) Rawsambl. For Rawsambl, we additionally report throughput (average number of signals analyzed per second per single CPU thread) to provide insights about its capabilities for real-time analysis. To measure performance and peak memory usage, we use the `time -v` command in Linux when running Rawsambl, minimap2, and Dorado. For average speedup and memory comparisons of Rawsambl against other methods, we use the geometric mean to reduce the impact of outlier data points on the average calculation.

We evaluate Rawsambl based on two use cases: 1) read overlapping and 2) *de novo* assembly. We generate read

overlaps from 1) raw signals using Rawsambl and 2) base-called sequences (with Dorado’s HAC model) of corresponding strands of raw signals using minimap2. To evaluate all-vs-all overlapping, we calculate the ratio of overlapping pairs 1) shared by both Rawsambl and minimap2, 2) unique to Rawsambl, and 3) unique to minimap2. For *de novo* assembly, we use miniasm [68] to assemble the read overlaps that Rawsambl and minimap2 generate in a PAF file. We use miniasm because it enables us to evaluate the impact of overlaps that Rawsambl and minimap2 finds by *using the same assembler* for both of them. To identify the roofline in terms of the assembly contiguity given a dataset, we use a highly accurate assembler as *gold standard* for our evaluations. To do this, we use Dorado’s most accurate model (i.e., SUP) to construct highly accurate reads and use Flye [81] to construct assemblies from these reads, as suggested in the guidelines by ONT [82]. This approach enables us to evaluate the gap between the assemblies that Rawsambl generates and the golden standard assembly that can be constructed from the same datasets.

To evaluate the assemblies constructed from the overlaps that Rawsambl and minimap2 generate, we use several metrics that are mainly related to the contiguity of the assemblies. These metrics are 1) the total length of unitigs (Total Length), 2) the number of nucleotides in the largest assembly graph component (Largest Comp.), 3) unitig length at which 50% of the assembly is covered by unitigs of equal or greater length (N50), 4) area under the Nx curve to generate a more robust evaluation of contiguity (auN) [83], 5) longest unitig length, and 6) the number of unitigs. We use Bandage [84] to visualize these assemblies.

We provide the parameter settings and versions for each tool as well as the details of the preset parameters in Rawsambl in Supplementary Tables S2 (parameters), S3 (details of presets), and S4 (versions). We provide the scripts to fully reproduce our results on the GitHub repository at <https://github.com/CMU-SAFARI/RawHash>, which contains the corresponding release version of Rawsambl we show in Supplementary Table S4. We provide the detailed reasoning behind the choice of Flye in order to generate the gold standard in Supplementary Material C.

3.2. Performance and Memory

Throughput. Table 2 shows the throughput (i.e., signals processed per second per CPU thread) that Rawsambl reports. Our goal is to estimate the number of CPU threads needed to achieve a throughput faster than the

throughput of a single sequencer. Using as few CPU threads as possible is useful to 1) provide better scalability (i.e., analyzing a larger amount of data with the same computation capabilities) and 2) reduce the overall computational requirements and corresponding energy consumption (i.e., analyzing the same amount of data with less computational capabilities). The latter is especially essential for resource-constrained devices (e.g., devices with external and limited batteries). The throughput of a single nanopore is around 5,000 signals per second [35], and the entire sequencer is usually equipped with 512 nanopores. This means a single sequencer’s throughput is around 2,560,000 signals per second ($5,000 \times 512$) [85]. We find that Rawsamle provides an average throughput of 2,432,561 signals per second **per CPU thread**. This means Rawsamle can achieve an analysis throughput faster than a single sequencer’s throughput by using an average of two CPU threads. This shows that the overlapping mechanism of Rawsamle is fast enough for performing real-time overlapping tasks using very few CPU threads.

Table 2: Rawsamle Throughput (signals processed per second per CPU thread).

	D1	D2	D3	D4	D5
	<i>SARS-CoV-2</i>	<i>E. coli</i>	<i>Yeast</i>	<i>Green Algae</i>	<i>Human</i>
Throughput	2,065,764	2,720,702	2,128,800	1,668,065	3,579,472

Computational resources. Table 3 shows the computational resources of the different approaches. Inside the parentheses provided with the minimap2 results, we provide the ratio between the reported result and the corresponding Rawsamle result (if higher than $1\times$, Rawsamle is better).

We make three key observations. First, Rawsamle provides a substantial speedup and lower peak memory usage compared to minimap2 when combined with Dorado’s fast model on a CPU by, on average, $16.36\times$ (elapsed time), $16.45\times$ (CPU time), and $11.73\times$ (peak memory usage). When using Dorado’s HAC model, Rawsamle provides even better results on average by $59.70\times$ (elapsed time), $36.93\times$ (CPU time), and $11.23\times$ (peak memory usage), since running the HAC model is computationally more costly than running the fast model.

Second, Rawsamle achieves an average: 1) speedup of $1.99\times$ (HAC) and $7.40\times$ (SUP), and 2) reduced peak memory usage of $1.53\times$ (HAC) and $1.70\times$ (SUP), compared to GPU-based basecalling followed by minimap2. Although basecalling with GPUs followed by overlapping is usually faster in most cases when using the HAC model (**Minimap2 + Dorado GPU (HAC)** in Table 3), Rawsam-

Table 3: Comparison of various tools across different organisms in terms of elapsed time, CPU time, and peak memory usage. The values in parentheses represent the ratio of the result shown in the cell compared to the corresponding result of Rawsamle (values higher than $1\times$ indicate that Rawsamle performs better). We highlight the cells that Rawsamle provide a **better and **worse** results with colors.**

Organism	Tool	Elapsed time (hh:mm:ss)	CPU time (sec)	Peak Mem. (GB)
D1 <i>SARS-CoV-2</i>	Rawsamle	0:00:03	33	1.07
	Minimap2	0:00:01 (0.33 \times)	19 (0.58 \times)	0.16 (0.15 \times)
	Minimap2 + Dorado CPU (Fast)	0:01:45 (35.00 \times)	3,227 (97.79 \times)	44.93 (41.99 \times)
	Minimap2 + Dorado CPU (HAC)	0:05:45 (115.00 \times)	5,457 (165.36 \times)	57.98 (54.19 \times)
	Minimap2 + Dorado GPU (HAC)	0:01:41 (33.67 \times)	NA	0.8 (0.75 \times)
	Minimap2 + Dorado GPU (SUP)	0:25:47 (515.67 \times)	NA	1.23 (1.15 \times)
D2 <i>E. coli</i>	Rawsamle	1:12:44	132,758	6.72
	Minimap2	0:14:25 (0.20 \times)	25,721 (0.19 \times)	26.73 (3.98 \times)
	Minimap2 + Dorado CPU (Fast)	7:17:05 (6.01 \times)	583,358 (4.39 \times)	50.43 (7.50 \times)
	Minimap2 + Dorado CPU (HAC)	32:26:12 (26.76 \times)	1,335,697 (10.06 \times)	38.0 (5.65 \times)
	Minimap2 + Dorado GPU (HAC)	0:36:14 (0.50 \times)	NA	26.73 (3.98 \times)
	Minimap2 + Dorado GPU (SUP)	1:30:30 (1.24 \times)	NA	26.73 (3.98 \times)
D3 <i>Yeast</i>	Rawsamle	0:01:18	2,241	6.39
	Minimap2	0:00:21 (0.27 \times)	290 (0.13 \times)	5.25 (0.82 \times)
	Minimap2 + Dorado CPU (Fast)	0:54:04 (41.59 \times)	71,796 (32.04 \times)	56.13 (8.78 \times)
	Minimap2 + Dorado CPU (HAC)	3:13:56 (149.18 \times)	193,640 (86.41 \times)	65.43 (10.24 \times)
	Minimap2 + Dorado GPU (HAC)	0:04:33 (3.50 \times)	NA	5.25 (0.82 \times)
	Minimap2 + Dorado GPU (SUP)	0:10:33 (8.12 \times)	NA	5.92 (0.93 \times)
D4 <i>Green Algae</i>	Rawsamle	0:07:57	14,064	8.67
	Minimap2	0:00:47 (0.10 \times)	882 (0.06 \times)	8.7 (1.00 \times)
	Minimap2 + Dorado CPU (Fast)	1:16:35 (9.63 \times)	79,606 (5.66 \times)	50.88 (5.87 \times)
	Minimap2 + Dorado CPU (HAC)	4:30:07 (33.98 \times)	286,362 (20.36 \times)	64.07 (7.39 \times)
	Minimap2 + Dorado GPU (HAC)	0:06:01 (0.76 \times)	NA	8.7 (1.00 \times)
	Minimap2 + Dorado GPU (SUP)	0:14:54 (1.87 \times)	NA	8.7 (1.00 \times)
D5 <i>Human</i>	Rawsamle	0:28:56	51,975	6.0
	Minimap2	0:01:52 (0.06 \times)	1,372 (0.03 \times)	20.21 (3.37 \times)
	Minimap2 + Dorado CPU (Fast)	6:42:24 (13.91 \times)	802,983 (15.45 \times)	81.98 (13.66 \times)
	Minimap2 + Dorado CPU (HAC)	23:27:18 (48.64 \times)	1,219,043 (23.45 \times)	46.12 (7.69 \times)
	Minimap2 + Dorado GPU (HAC)	0:20:24 (0.71 \times)	NA	20.31 (3.38 \times)
	Minimap2 + Dorado GPU (SUP)	1:05:48 (2.27 \times)	NA	20.21 (3.37 \times)

le still achieves better average speedup due to the substantial speedup it provides for the D1 dataset. Although comparing the results between CPUs and GPUs is not ideal due to the massive parallelism that GPUs provide compared to CPUs, Rawsamle still provides comparable and even better performance even with the limited parallelism (i.e., 32 threads) it uses on CPUs compared to the parallelism that GPUs provide (e.g., a few tens of thousands of threads). This shows that Rawsamle can provide even faster results when accelerated with GPUs (outside the scope of this work) based on its comparison when basecalling is done using CPUs and GPUs.

Third, minimap2, without considering the resources that basecalling requires, is more resource-efficient than Rawsamle as it takes on average $0.16\times$ (elapsed time), $0.12\times$ (CPU time), and $1.11\times$ (peak memory usage) of those Rawsamle takes. This is mainly expected as analyzing raw signals requires additional steps (e.g., signal-to-event conversion), more memory due to sequencing depth (as opposed to a reference genome), and incurs noise that requires less efficient parameter settings for Rawsamle (e.g., the window parameter in minimizers) when analyzing raw signals compared to minimap2. Fu-

ture work can focus on processing these raw signals more accurately to reduce the limits for adjusting parameters that can impact performance and memory usage.

We conclude that Rawsamble can perform read overlapping with higher throughput that can be useful when focusing on real-time analysis and better computational resources than CPU-based basecalling followed by minimap2. We find that Rawsamble’s speed is mainly dependent on the amount of bases stored in the hash table, as the speed decreases with increasing the number of locations that need to be analyzed in the index per read. To resolve this scalability issue, future work should focus on designing indexing and filtering methods that provide a limitation on the volume of signals stored in the index and processed during the overlapping step. These results can also be useful when basecalling raw signals using GPUs to reduce the computational overhead that GPU-based basecalling requires, which we discuss in Section 4.

3.3. All-vs-All Overlapping Statistics

Table 4 shows the all-vs-all overlapping statistics between Rawsamble and minimap2, where each row sums to 100%. We make two key observations. First, on average, 36.57% of overlap pairs generated by Rawsamble are shared with the overlap pairs that minimap2 generates. This shows that a large fraction of overlapping pairs does not require basecalling to generate identical overlapping information identified by minimap2 after basecalling. Second, although Rawsamble can find a substantial amount of overlap pairs identical to the overlaps minimap2 finds, specifically for the D1 dataset, there are still overlapping pairs unique to Rawsamble (16.25% on average) and minimap2 (47.17% on average), mainly due to the decreased shared overlaps as the genome size increases. These differences are likely due to differences in 1) certain parameters (e.g., chaining scores) and 2) increased noise inherent in raw signals compared to basecalled sequences, which can become more pronounced in genomes with greater size, complexity, or repetitiveness. Additionally, as observed in an earlier work [86], constructing contiguous assemblies is not dependent on finding as many overlapping pairs as possible. Instead, contiguous assemblies can still be constructed using a smaller but useful portion of overlapping pairs. We conclude that Rawsamble provides a mechanism that shares a large portion of overlaps with minimap2, while the shared portions decrease as the genome size increases.

Table 4: All-vs-all Overlapping Statistics. Percentages show the overlapping pairs that are 1) unique to Rawsamble, 2) unique to minimap2, and 3) reported in both tools (Shared Overlaps).

	Organism	Unique to Rawsamble (%)	Unique to Minimap2 (%)	Shared Overlaps (%)
D1	<i>SARS-CoV-2</i>	11.55	15.27	73.18
D2	<i>E. coli</i>	8.33	50.62	41.05
D3	<i>Yeast</i>	24.94	35.17	39.89
D4	<i>Green Algae</i>	3.76	78.64	17.61
D5	<i>Human</i>	32.69	56.18	11.13

3.4. De novo Assembly Evaluations

To evaluate the impact of differing reported overlaps between Rawsamble and minimap2, we construct *de novo* assemblies from these overlaps. Table 5 shows the statistics of these *de novo* assemblies. We do not provide the assembly statistics for the D1 dataset as miniasm cannot generate an assembly using the overlaps from Rawsamble and minimap2, potentially due to the small size of the genome. We make three observations.

First, we find that the overlaps found using Rawsamble can form long paths during assembly that lead to assembly constructions and large connected components. **Rawsamble is the first work that enables *de novo* assembly construction directly from raw signal overlaps without basecalling**, which has several implications and can enable future work, as we discuss in Section 4.

Second, we observe that the unitigs generated from Rawsamble overlaps are usually less contiguous compared to those generated from minimap2 overlaps, based on all the metrics we show in Table 5 and Supplementary Figures S2–S5. Compared to the gold standard assemblies generated using highly accurate basecalled reads and a state-of-the-art assembler, we find that Rawsamble can still achieve a significant portion of the assembly contiguity, especially for the D2 dataset (*E.coli*). For example, Rawsamble constructs unitigs with the longest unitig length of 2.7 million bases, which is over half the length of the *E. coli* genome, whereas the gold standard assembly produces a single unitig covering the entire genome. **This indicates that Rawsamble can achieve substantial contiguity relative to the gold standard without basecalling.**

Third, for the larger genomes in the D4 and D5 datasets, we find that Rawsamble can construct longer unitigs compared to those generated by minimap2 and, notably, achieves better contiguity than the gold standard assem-

blies in the D5 dataset. The coverage of these datasets is substantially lower than that of other datasets. This suggests that Rawsamble can find more useful overlaps leading to longer paths in the assembly for the cases when coverage is relatively lower (e.g., coverage of less than or around $5\times$ in Table 1). Basecalled sequences may generate more contiguous assemblies when the coverage is higher. We conclude that Rawsamble generates useful overlapping information, enabling the construction of assemblies directly from raw signals. This approach achieves substantial contiguity and, in some cases (e.g., at low coverage), provides superior contiguity compared to minimap2 and gold standard assemblies.

Table 5: Assembly Statistics.

Dataset	Tool	Total Length (bp)	Largest Comp. (bp)	N50 (bp)	auN (bp)	Longest Unitig (bp)	Unitig Count
D2 <i>E. coli</i>	Rawsamble	14,525,505	4,841,669	1,535,079	1,309,738	2,722,499	31
	minimap2	10,434,542	5,207,206	5,204,754	5,194,738	5,207,206	4
	Gold standard	5,235,343	5,235,343	5,235,343	5,235,343	5,235,343	1
D3 <i>Yeast</i>	Rawsamble	13,898,208	362,050	41,118	48,106	161,883	396
	minimap2	23,755,455	1,611,876	134,050	150,908	464,054	282
	Gold standard	11,963,521	11,835,059	640,934	623,210	1,073,346	68
D4 <i>Green Algae</i>	Rawsamble	3,448,899	448,422	93,111	108,818	252,038	50
	minimap2	2,117,190	198,709	63,310	88,906	198,709	55
	Gold standard	106,479,288	2,255,807	452,774	538,136	1,667,975	420
D5 <i>Human</i>	Rawsamble	1,850,419	493,004	51,300	116,049	364,113	48
	minimap2	747,607	65,951	19,476	22,103	48,424	61
	Gold standard	8,365,210	367,305	19,329	29,697	150,470	592

4. Discussion and Future Work

Limitations. Our evaluation demonstrates that Rawsamble achieves high throughput, making it a viable candidate for real-time analysis while constructing *de novo* assemblies. However, there are still two main challenges to fully utilize real-time *de novo* assembly construction during sequencing. First, the hash-based index should be constructed and updated dynamically in real-time while sequencing is in progress. Although Rawsamble provides the mechanisms for storing multiple hash tables that can be constructed for each chunk of raw signals generated in real-time, it is not computationally feasible to dynamically update the index for all sequenced signals as the memory and computational burden increases with each hash table generated. Such an approach requires a decision-making mechanism to dynamically stop updating the index after sequencing a certain amount of signals. The stopping mechanism should be accurate enough to ensure that the current state of the index provides sufficient information to find the overlaps between the already sequenced signals and the new signals generated after the index construction. Second, the assembly graph should be constructed and updated dynamically while the new overlap information is generated in real time. This is challenging as the intermediate steps for generating the unitigs (e.g., the transitive reduction step [87]) in

assembly graphs may not work optimally without the full overlap information, as it is likely to remove graph connections that can be useful with new overlap information. It might be feasible to use graph structures that are more suitable for streaming data generation, such as de Bruijn graphs, for assembly construction purposes [88–90].

Rawsamble can find overlaps only between reads coming from the same strand, as it lacks the capability to construct the reverse complemented version of the signals to identify the matches on the other strands. This potentially leads to gaps in the assembly and construction of the unitigs from both strands. Designing a mechanism that can reverse complement raw signals without basecalling is future work.

We evaluate Rawsamble using raw signals generated from ONT’s R9.4 flowcells to show that overlapping information between raw signals can be used to construct *de novo* assemblies. We leave optimizations for newer flow cell versions (e.g., R10.4.1) for future work.

New Directions for Future Work. We identify several new directions for future work. First, integrating the overlapping information with basecalling can provide accuracy benefits for basecallers. Existing basecallers are designed to basecall individual reads without such overlapping information. Such a combined approach can provide additional useful features for the underlying machine learning models in basecallers to improve the basecalling accuracy. Second, *de novo* assembly construction enables identifying the reads that do not provide useful information for assembly if they are fully contained by other overlapping read pairs [68]. Identifying these potentially useless reads early on provides the opportunity to avoid basecalling them, which can improve the overall execution time of basecalling by filtering out such reads. Third, *de novo* assembly construction from raw signals provides new opportunities to design new basecallers that can basecall the assembled signals. Such a basecaller has the potential to substantially improve the performance, as it enables basecalling fewer long unitigs instead of many shorter reads.

While Rawsamble enables new directions in raw signal analysis, particularly for *de novo* assembly, several challenges and opportunities for future work remain. Addressing these challenges has the potential to enable new use cases and applications in raw signal and basecalled sequence analyses.

5. Conclusion

We introduce Rawsamble, the *first* mechanism that can find overlaps between two sets of raw nanopore signals

without translating them to bases. We find that Rawsam- ble can 1) find overlaps while meeting the real-time re- quirements with an average throughput of 2,432,561 sig- nals/sec per CPU thread, 2) reduce the overall time needed for finding overlaps (on average by $16.36\times$ and up to by $41.59\times$) and peak memory usage (on average by $11.73\times$ and up to by $41.99\times$) compared to the time and memory needed to run state-of-the-art read mapper (minimap2) combined with the Dorado basecaller running on a CPU with its fastest model, 3) share a large portion of overlap- ping pairs with minimap2 (36.57% on average), and 4) con- struct long assemblies from these useful overlaps. We find that we can construct assemblies of half the length of the entire *E. coli* genome (i.e., of length 2.7 million bases) directly from raw signal overlaps without base- calling. Finding overlapping pairs from raw signals is critical for enabling new directions that have not been explored before for raw signal analysis, such as *de novo* assembly construction from overlaps that we explore in this work. We discuss many other new directions that can be enabled by finding overlaps and constructing *de novo* assemblies.

We hope and believe that Rawsam- ble enables future work in at least two key directions. First, we aim to fully perform end-to-end genome analysis without basecalling. This can be achieved by further improving tools such as Rawsam- ble to construct *de novo* assemblies directly from raw signals such that these assemblies are consistently better than those generated from basecalled sequences in all cases. Second, we should rethink how we train and use modern neural network-based basecallers by integrating additional useful information (e.g., overlaps or assemblies of signals) generated by Rawsam- ble into these basecallers.

Acknowledgments

SAFARI Research Group acknowledges the generous gift funding provided by our industrial partners (especially by Google, Huawei, Intel, Microsoft, VMware), which has been instrumental in enabling the 15+ year-long research SAFARI Research Group has been conducting on accel- erating genome analysis. This work is also partially sup- ported by the Semiconductor Research Corporation (SRC), the European Union’s Horizon programme for research and innovation [101047160 - BioPIM] and the Swiss Na- tional Science Foundation (SNSF) [200021_213084]. M.M. has been supported by the Max Planck ETH Center for Learning Systems and by SNF Project Grant #200550 to A.K. S.G. is funded through Swiss National Science Foun- dation Project grant no. 200550 to A.K.

References

- [1] G. Menestrina, “Ionic channels formed by *Staphylococcus aureus* alpha- toxin: Voltage-dependent inhibition by divalent and trivalent cations,” *The Journal of Membrane Biology*, vol. 90, no. 2, pp. 177–190, Jun. 1986.
- [2] G. M. Cherf *et al.*, “Automated forward and reverse ratcheting of DNA in a nanopore at 5-Å precision,” *Nature Biotechnology*, vol. 30, no. 4, pp. 344–348, Apr. 2012.
- [3] E. A. Manrao *et al.*, “Reading DNA at single-nucleotide resolution with a mutant MspA nanopore and phi29 DNA polymerase,” *Nature Biotechnology*, vol. 30, no. 4, pp. 349–353, Apr. 2012.
- [4] A. H. Laszlo *et al.*, “Decoding long nanopore sequencing reads of natural DNA,” *Nature Biotechnology*, vol. 32, no. 8, pp. 829–833, Aug. 2014.
- [5] D. Deamer *et al.*, “Three decades of nanopore sequencing,” *Nature Biotech- nology*, vol. 34, no. 5, pp. 518–524, May 2016.
- [6] J. J. Kasianowicz *et al.*, “Characterization of individual polynucleotide molecules using a membrane channel,” *Proceedings of the National Academy of Sciences*, vol. 93, no. 24, pp. 13 770–13 773, Nov. 1996.
- [7] A. Meller *et al.*, “Rapid nanopore discrimination between single polynu- cleotide molecules,” *Proceedings of the National Academy of Sciences*, vol. 97, no. 3, pp. 1079–1084, Feb. 2000.
- [8] D. Stoddart *et al.*, “Single-nucleotide discrimination in immobilized DNA oligonucleotides with a biological nanopore,” *Proceedings of the National Academy of Sciences*, vol. 106, no. 19, pp. 7702–7707, May 2009.
- [9] A. H. Laszlo *et al.*, “Detection and mapping of 5-methylcytosine and 5- hydroxymethylcytosine with nanopore MspA,” *Proceedings of the National Academy of Sciences*, vol. 110, no. 47, pp. 18 904–18 909, Nov. 2013.
- [10] J. Schreiber *et al.*, “Error rates for nanopore discrimination among cytosine, methylcytosine, and hydroxymethylcytosine along individual DNA strands,” *Proceedings of the National Academy of Sciences*, vol. 110, no. 47, pp. 18 910–18 915, Nov. 2013.
- [11] T. Z. Butler *et al.*, “Single-molecule DNA detection with an engineered MspA protein nanopore,” *Proceedings of the National Academy of Sciences*, vol. 105, no. 52, pp. 20 647–20 652, Dec. 2008.
- [12] I. M. Derrington *et al.*, “Nanopore DNA sequencing with MspA,” *Proceed- ings of the National Academy of Sciences*, vol. 107, no. 37, pp. 16 060–16 065, Sep. 2010.
- [13] L. Song *et al.*, “Structure of Staphylococcal α -Hemolysin, a Heptameric Transmembrane Pore,” *Science*, vol. 274, no. 5294, pp. 1859–1865, Dec. 1996.
- [14] B. Walker *et al.*, “A pore-forming protein with a metal-actuated switch,” *Protein Engineering, Design and Selection*, vol. 7, no. 5, pp. 655–662, May 1994.
- [15] Z. L. Wescoe *et al.*, “Nanopores Discriminate among Five C5-Cytosine Variants in DNA,” *Journal of the American Chemical Society*, vol. 136, no. 47, pp. 16 582–16 587, Nov. 2014.
- [16] K. R. Lieberman *et al.*, “Processive Replication of Single DNA Molecules in a Nanopore Catalyzed by phi29 DNA Polymerase,” *Journal of the American Chemical Society*, vol. 132, no. 50, pp. 17 961–17 972, Dec. 2010.
- [17] S. M. Bezrukov *et al.*, “Dynamics and Free Energy of Polymers Partitioning into a Nanoscale Pore,” *Macromolecules*, vol. 29, no. 26, pp. 8517–8522, Jan. 1996.
- [18] M. Akeson *et al.*, “Microsecond Time-Scale Discrimination Among Poly- cytidylic Acid, Polyadenylic Acid, and Polyuridylic Acid as Homopolymers or as Segments Within Single RNA Molecules,” *Biophysical Journal*, vol. 77, no. 6, pp. 3227–3233, Dec. 1999.
- [19] D. Stoddart *et al.*, “Nucleobase Recognition in ssDNA at the Central Con- striction of the α -Hemolysin Pore,” *Nano Letters*, vol. 10, no. 9, pp. 3633–3637, Sep. 2010.
- [20] N. Ashkenasy *et al.*, “Recognizing a Single Base in an Individual DNA Strand: A Step Toward DNA Sequencing in Nanopores,” *Angewandte Chemie International Edition*, vol. 44, no. 9, pp. 1401–1404, Feb. 2005.
- [21] D. Stoddart *et al.*, “Multiple Base-Recognition Sites in a Biological Nanopore: Two Heads are Better than One,” *Angewandte Chemie Inter- national Edition*, vol. 49, no. 3, pp. 556–559, Jan. 2010.
- [22] S. M. Bezrukov and J. J. Kasianowicz, “Current noise reveals protonation kinetics and number of ionizable sites in an open protein ion channel,” *Physical Review Letters*, vol. 70, no. 15, pp. 2352–2355, Apr. 1993.
- [23] J.-Y. Zhang *et al.*, “A single-molecule nanopore sequencing platform,” *bioRxiv*, p. 2024.08.19.608720, 2024.
- [24] M. Jain *et al.*, “Nanopore sequencing and assembly of a human genome with ultra-long reads,” *Nature Biotechnology*, vol. 36, no. 4, pp. 338–345, Apr. 2018.
- [25] J. Pugh, “The Current State of Nanopore Sequencing,” in *Nanopore Se- quencing: Methods and Protocols*, K. Arakawa, Ed. New York, NY: Springer US, 2023, pp. 3–14.
- [26] D. Senol Cali *et al.*, “Nanopore sequencing technology and tools for genome assembly: computational analysis of the current state, bottle- necks and future directions,” *Briefings in Bioinformatics*, vol. 20, no. 4, pp. 1542–1559, Jul. 2019.

- [27] M. Loose *et al.*, “Real-time selective sequencing using nanopore technology,” *Nature Methods*, vol. 13, no. 9, pp. 751–754, Sep. 2016.
- [28] R. Flynn *et al.*, “Evaluation of nanopore sequencing for epigenetic epidemiology: a comparison with DNA methylation microarrays,” *Hum. Mol. Genet.*, 2022.
- [29] B. Bloemen *et al.*, “Development of a portable on-site applicable metagenomic data generation workflow for enhanced pathogen and antimicrobial resistance surveillance,” *Sci. Rep.*, 2023.
- [30] M. B. Cavlak *et al.*, “TargetCall: Eliminating the Wasted Computation in Basecalling via Pre-Basecalling Filtering,” *Frontiers in Genetics*, Sep. 2024.
- [31] Z. Xu *et al.*, “Fast-bonito: A Faster Deep Learning Based Basecaller for Nanopore Sequencing,” *Artificial Intelligence in the Life Sciences*, vol. 1, p. 100011, 2021, publisher: Elsevier.
- [32] P. Perešini *et al.*, “Nanopore base calling on the edge,” *Bioinformatics*, 2021.
- [33] V. Boža *et al.*, “DeepNano: Deep recurrent neural networks for base calling in MinION nanopore reads,” *PLOS One*, 2017.
- [34] V. Boža *et al.*, “DeepNano-blitz: a fast base caller for MinION nanopore sequencers,” *Bioinformatics*, vol. 36, no. 14, pp. 4191–4192, Jul. 2020.
- [35] Oxford Nanopore Technologies, “Dorado,” 2024. [Online]. Available: <https://github.com/nanoporetech/dorado>
- [36] Oxford Nanopore Technologies, “Guppy,” 2017.
- [37] X. Lv *et al.*, “An end-to-end Oxford nanopore basecaller using convolution-augmented transformer,” in *BIBM*, 2020.
- [38] G. Singh *et al.*, “RUBICON: a framework for designing efficient deep learning-based genomic basecallers,” *Genome Biology*, 2024.
- [39] Y.-z. Zhang *et al.*, “Nanopore basecalling from a perspective of instance segmentation,” *BMC Bioinformatics*, vol. 21, no. 3, p. 136, Apr. 2020.
- [40] X. Xu *et al.*, “Lokatt: a hybrid DNA nanopore basecaller with an explicit duration hidden Markov model and a residual LSTM network,” *BMC Bioinformatics*, vol. 24, no. 1, p. 461, Dec. 2023.
- [41] J. Zeng *et al.*, “Causalcall: Nanopore Basecalling Using a Temporal Convolutional Network,” *Frontiers in Genetics*, vol. 10, 2020.
- [42] H. Teng *et al.*, “Chiron: translating nanopore raw signal directly into nucleotide sequence using deep learning,” *GigaScience*, vol. 7, no. 5, p. giy037, May 2018.
- [43] H. Konishi *et al.*, “Halcyon: an accurate basecaller exploiting an encoder–decoder model with monotonic attention,” *Bioinformatics*, vol. 37, no. 9, pp. 1211–1217, Jun. 2021.
- [44] Y.-M. Yeh and Y.-C. Lu, “MSRCall: a multi-scale deep neural network to basecall Oxford Nanopore sequences,” *Bioinformatics*, vol. 38, no. 16, pp. 3877–3884, Aug. 2022.
- [45] B. Noordijk *et al.*, “baseLess: lightweight detection of sequences in raw MinION data,” *Bioinformatics Advances*, vol. 3, no. 1, p. vbad017, Jan. 2023.
- [46] N. Huang *et al.*, “SACall: A Neural Network Basecaller for Oxford Nanopore Sequencing Data Based on Self-Attention Mechanism,” *IEEE/ACM Transactions on Computational Biology and Bioinformatics*, vol. 19, no. 1, pp. 614–623, 2022.
- [47] N. Miculinic *et al.*, “MinCall - MinION end2end convolutional deep learning basecaller,” *arXiv*, 2019.
- [48] N. J. Loman *et al.*, “A complete bacterial genome assembled de novo using only nanopore sequencing data,” *Nature Methods*, vol. 12, no. 8, pp. 733–735, Aug. 2015.
- [49] M. David *et al.*, “Nanocall: an open source basecaller for Oxford Nanopore sequencing data,” *Bioinformatics*, vol. 33, no. 1, pp. 49–55, Jan. 2017.
- [50] W. Timp *et al.*, “DNA Base-Calling from a Nanopore Using a Viterbi Algorithm,” *Biophysical Journal*, 2012.
- [51] J. Schreiber and K. Karplus, “Analysis of nanopore data using hidden Markov models,” *Bioinformatics*, vol. 31, no. 12, pp. 1897–1903, Jun. 2015.
- [52] Y. Bao *et al.*, “SquiggleNet: real-time, direct classification of nanopore signals,” *Genome Biology*, vol. 22, no. 1, p. 298, Oct. 2021.
- [53] H. Zhang *et al.*, “Real-time mapping of nanopore raw signals,” *Bioinformatics*, vol. 37, no. Supplement_1, pp. i477–i483, Jul. 2021.
- [54] S. Kovaka *et al.*, “Targeted nanopore sequencing by real-time mapping of raw electrical signal with UNCALLED,” *Nature Biotechnology*, vol. 39, no. 4, pp. 431–441, Apr. 2021.
- [55] A. Senanayake *et al.*, “DeepSelectNet: deep neural network based selective sequencing for oxford nanopore sequencing,” *BMC Bioinformatics*, vol. 24, no. 1, p. 31, Jan. 2023.
- [56] Sam Kovaka *et al.*, “Uncalled4 improves nanopore DNA and RNA modification detection via fast and accurate signal alignment,” *bioRxiv*, 2024.
- [57] J. Lindegger *et al.*, “RawAlign: Accurate, Fast, and Scalable Raw Nanopore Signal Mapping via Combining Seeding and Alignment,” *arXiv*, 2023.
- [58] C. Firtina *et al.*, “RawHash: enabling fast and accurate real-time analysis of raw nanopore signals for large genomes,” *Bioinform.*, 2023.
- [59] C. Firtina *et al.*, “RawHash2: Mapping Raw Nanopore Signals Using Hash-Based Seeding and Adaptive Quantization,” *Bioinform.*, 2024.
- [60] P. J. Shih *et al.*, “Efficient real-time selective genome sequencing on resource-constrained devices,” *GigaScience*, 2023.
- [61] H. Sadasivan *et al.*, “Rapid Real-time Squiggle Classification for Read Until Using RawMap,” *Arch. Clin. Biomed. Res.*, 2023.
- [62] T. Dunn *et al.*, “SquiggleFilter: An accelerator for portable virus detection,” in *MICRO*, 2021.
- [63] V. S. Shivakumar *et al.*, “Sigmoni: classification of nanopore signal with a compressed pangome index,” *Bioinform.*, 2024.
- [64] H. Sadasivan *et al.*, “Accelerated Dynamic Time Warping on GPU for Selective Nanopore Sequencing,” *Journal of Biotechnology and Biomedicine*, vol. 7, pp. 137–148, 2024.
- [65] H. Gamaarachchi *et al.*, “GPU accelerated adaptive banded event alignment for rapid comparative nanopore signal analysis,” *BMC Bioinformatics*, vol. 21, no. 1, p. 343, Aug. 2020.
- [66] S. Samarasinghe *et al.*, “Energy Efficient Adaptive Banded Event Alignment using OpenCL on FPGAs,” in *ICIAFS*, 2021, pp. 369–374.
- [67] R. D. Fleischmann *et al.*, “Whole-Genome Random Sequencing and Assembly of *Haemophilus influenzae* Rd,” *Science*, vol. 269, no. 5223, pp. 496–512, Jul. 1995.
- [68] H. Li, “Minimap and miniasm: fast mapping and de novo assembly for noisy long sequences,” *Bioinformatics*, vol. 32, no. 14, pp. 2103–2110, Jul. 2016.
- [69] C. Firtina *et al.*, “BLEND: a fast, memory-efficient and accurate mechanism to find fuzzy seed matches in genome analysis,” *NAR Genomics and Bioinformatics*, vol. 5, no. 1, p. lqad004, Mar. 2023.
- [70] S. Bhattacharya *et al.*, “Molecular Dynamics Study of MspA Arginine Mutants Predicts Slow DNA Translocations and Ion Current Blockades Indicative of DNA Sequence,” *ACS Nano*, vol. 6, no. 8, pp. 6960–6968, Aug. 2012.
- [71] R. Kawano *et al.*, “Controlling the Translocation of Single-Stranded DNA through a-Hemolysin Ion Channels Using Viscosity,” *Langmuir*, vol. 25, no. 2, pp. 1233–1237, Jan. 2009.
- [72] R. M. M. Smeets *et al.*, “Noise in solid-state nanopores,” *Proceedings of the National Academy of Sciences*, vol. 105, no. 2, pp. 417–421, Jan. 2008.
- [73] H. Li, “Minimap2: pairwise alignment for nucleotide sequences,” *Bioinformatics*, vol. 34, no. 18, pp. 3094–3100, Sep. 2018.
- [74] J. T. Simpson *et al.*, “ABySS: A parallel assembler for short read sequence data,” *Genome Research*, 2009.
- [75] I. Sović *et al.*, “Approaches to DNA de novo assembly,” in *MIPRO*, 2013.
- [76] H. Li, “GFA: Graphical Fragment Assembly (GFA) Format Specification,” 2023. [Online]. Available: <https://github.com/GFA-spec/GFA-spec>
- [77] S. Mercogliano, “Rawasm,” 2024. [Online]. Available: <https://github.com/CMU-SAFARI/rawasm>
- [78] H. Gamaarachchi *et al.*, “Fast nanopore sequencing data analysis with SLOW5,” *Nat. Biotechnol.*, 2022.
- [79] “NVIDIA RTX A6000,” 2024. [Online]. Available: <https://www.nvidia.com/en-us/design-visualization/rtx-a6000>
- [80] “Intel® Xeon® Gold 6226R Processor,” 2024. [Online]. Available: <https://www.intel.com/content/www/us/en/products/sku/199347/in-tel-xeon-gold-6226r-processor-22m-cache-2-90-ghz/specifications.html>
- [81] M. Kolmogorov *et al.*, “Assembly of long, error-prone reads using repeat graphs,” *Nature Biotechnology*, vol. 37, no. 5, pp. 540–546, May 2019.
- [82] Oxford Nanopore Technologies, “Human assembly workflow,” 2022. [Online]. Available: <https://a.storyblok.com/f/196663/cd1c1c07ec/human-assembly-workflow.pdf>
- [83] H. Li, “aun: a new metric to measure assembly contiguity,” 2020. [Online]. Available: <https://lh3.github.io/2020/04/08/a-new-metric-on-assembly-contiguity>
- [84] R. R. Wick *et al.*, “Bandage: interactive visualization of de novo genome assemblies,” *Bioinform.*, 2015.
- [85] A. Magi *et al.*, “Nanopore sequencing data analysis: state of the art, applications and challenges,” *Briefings in Bioinformatics*, 2018.
- [86] R. Vaser and M. Šikić, “Time- and memory-efficient genome assembly with Raven,” *Nature Computational Science*, vol. 1, no. 5, pp. 332–336, May 2021.
- [87] E. W. Myers, “The fragment assembly string graph,” *Bioinform.*, 2005.
- [88] S. El-Metwally *et al.*, “LightAssembler: fast and memory-efficient assembly algorithm for high-throughput sequencing reads,” *Bioinform.*, 2016.
- [89] R. Rozov *et al.*, “Faucet: streaming de novo assembly graph construction,” *Bioinform.*, 2018.
- [90] C. Scott, “Streaming Methods for Assembly Graph Analysis,” Ph.D., University of California, Davis, 2022.

Supplementary Material for Rawsample: Overlapping and Assembling Raw Nanopore Signals using a Hash-based Seeding Mechanism

A. RawHash2 Overview

Rawsample builds improvements over RawHash2 [1,2], a mechanism that provides a hash-based similarity identification between a raw signal and a reference genome. We show the overview of RawHash2 in Supplementary Figure S1. RawHash2 has four key steps.

First, to generate sequences of signals that can be compared to each other, RawHash2 generates signals of k-mers, called *events*, from both a reference genome and raw signals. To generate events from reference genomes, it uses a lookup table, called *k-mer model*, that provides the expected signal value (i.e., event value) as a floating value for each possible k-mer where k is usually 6 or 9, depending on the flow cell version. To identify events (i.e., k-mers) in raw signals, RawHash2 performs a segmentation technique to detect the abrupt changes in signals, which enables identifying the regions in signals generated when sequencing a particular k-mer. RawHash2 uses the average value of signals within the same region as an event value after identifying outliers within the region. Due to the variations and noise in nanopore sequencing, event values generated from the same k-mer can slightly differ from each other, making it challenging to directly match the event values to each other to identify matching k-mers between a reference genome and raw signals.

Second, to mitigate this noise issue, RawHash2 quantizes the event values such that slightly different event values can be quantized into the same value (i.e., bucketing) to enable direct matching of quantized event values between a reference genome and raw signals. To enable an accurate quantization, RawHash2 identifies the range of values that are assigned to the same quantized value dynamically according to the nanopore model.

Third, to reduce the number of potential matches without reducing accuracy, RawHash2 concatenates the quantized event values of consecutive events (i.e., consecutive k-mers) and generates a hash value from these concatenated values.

Fourth, for the reference genome, these hash values are stored in a hash table along with their position information, which is usually known as the indexing step in read mapping. RawHash2 uses the hash values of raw signals to query the previously constructed hash table to identify matching hash values, known as *seed hits*, between a reference genome and a raw signal. Seed hits are used to identify chains of seed matches within proximity using the chaining algorithm proposed in minimap2 [3]. RawHash2 identifies the best chain among many chains based on a weighted decision strategy that takes several metrics into account, such as chaining score and mapping quality. RawHash2 uses the best chain as the best mapping for a read and reports a single mapping per read.

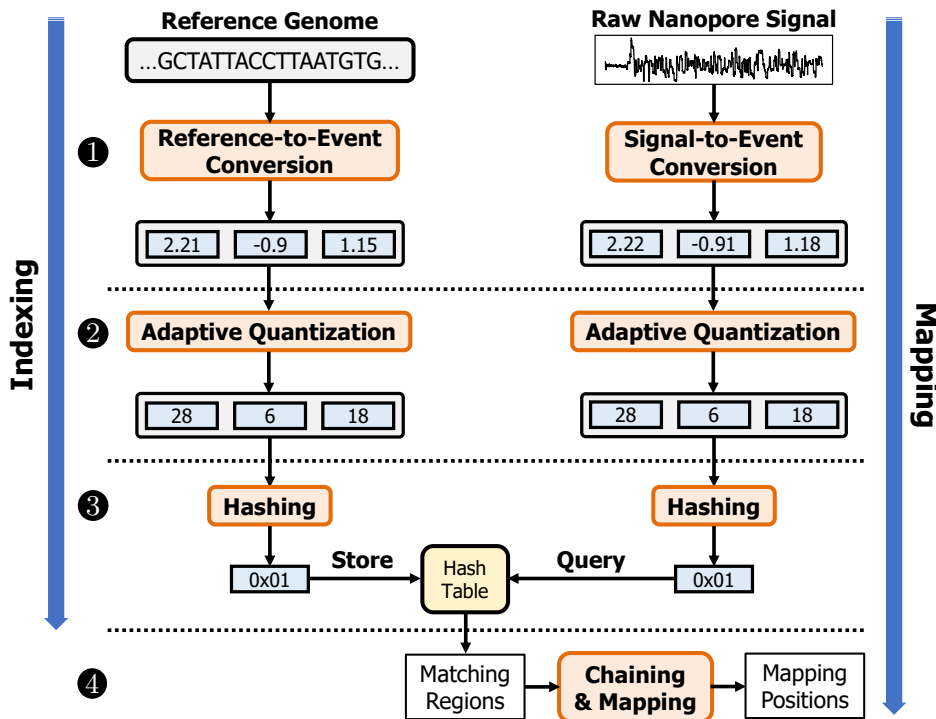


Figure S1: Overview of RawHash2.

B. Visualizing Assemblies

Supplementary Figures S2, S3, S4, and S5 show the assembly graphs created with miniasm in GFA formats. To construct these assembly graphs with miniasm, we provide the overlap information that Rawsambl and minimap2 provide as a PAF file [4]. We use Bandage [5] to visualize these assembly graphs. To provide the scale between unitigs generated using the same dataset, we annotate the longest contig in each assembly graph with their lengths.

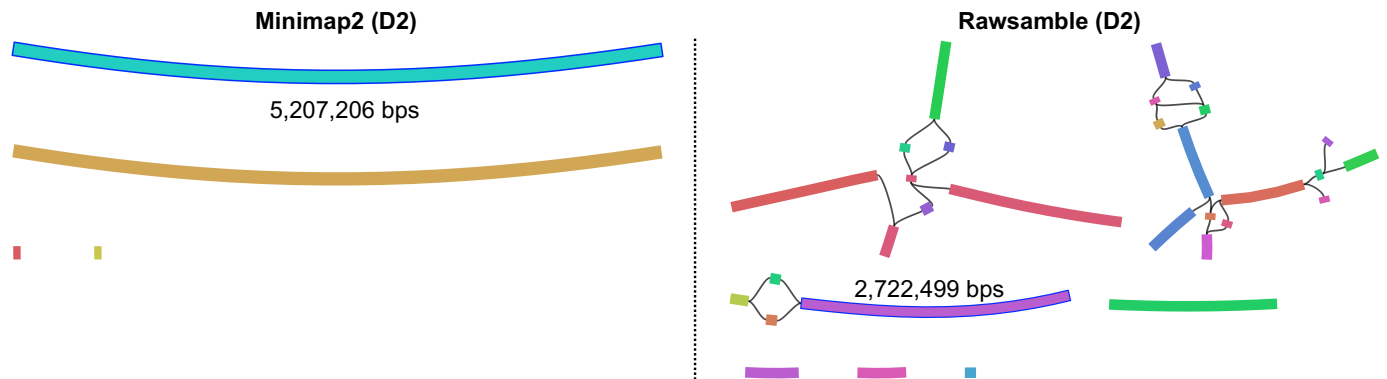


Figure S2: Visualization of the assembly graphs generated using Rawsambl and minimap2 overlaps from the D2 (*E. coli*) dataset.

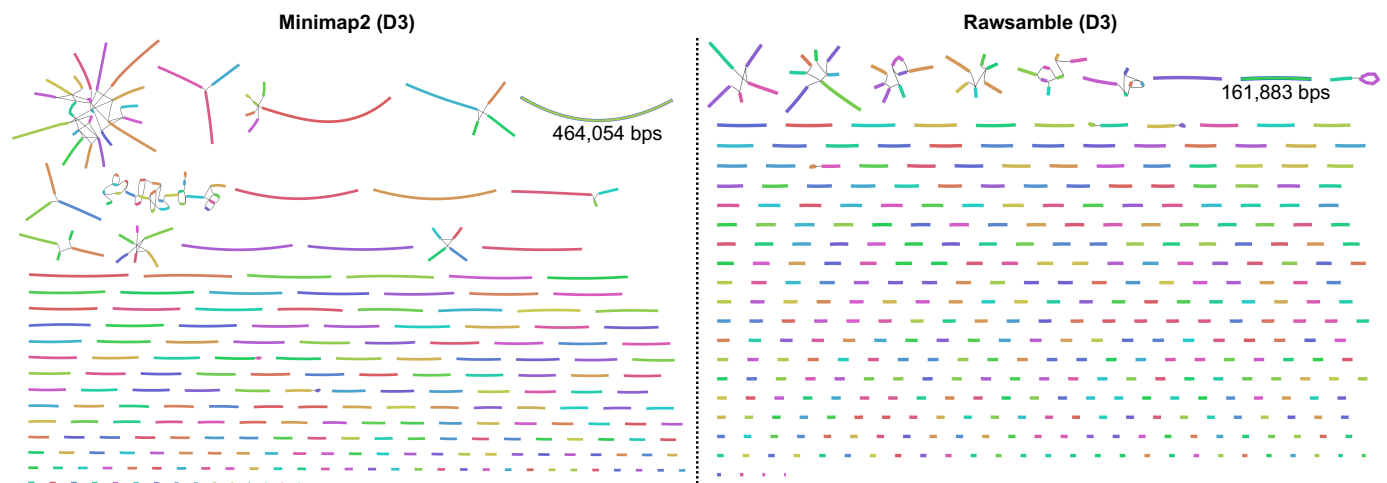


Figure S3: Visualization of the assembly graphs generated using Rawsambl and minimap2 overlaps from the D3 (*Yeast*) dataset.

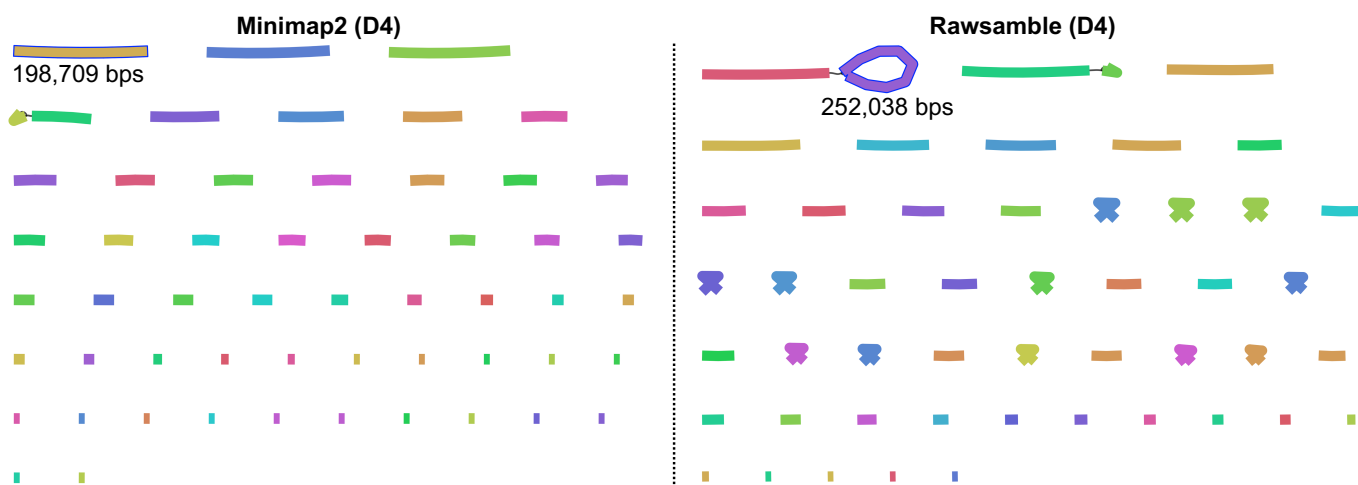


Figure S4: Visualization of the assembly graphs generated using Rawsamble and minimap2 overlaps from the D4 (*Green Algae*) dataset.

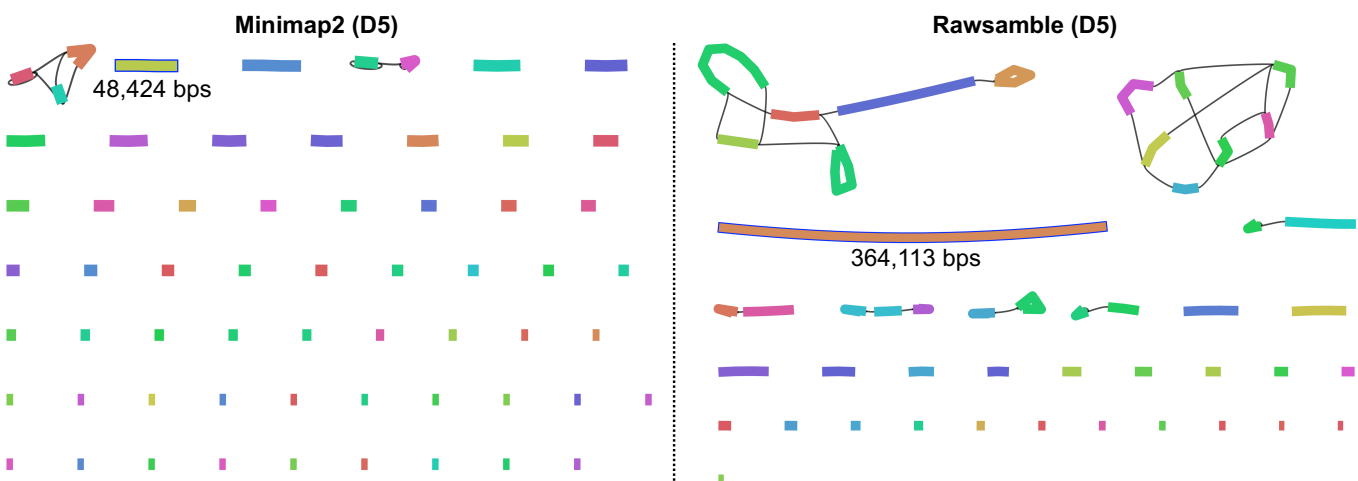


Figure S5: Visualization of the assembly graphs generated using Rawsamble and minimap2 overlaps from the D5 (*Human*) dataset.

C. Generating a Gold Standard Assembly

To generate a gold standard assembly using R9.4 Simplex reads, we explore two approaches.

First, we use the raw basecalled sequences directly with a set of state-of-the-art assemblers identified from recent benchmarks [6–9], namely Hifiasm [10], Verkko [11], LJA [12], HiCanu [13], and Flye [14].

Second, we apply error correction to the reads using the HERRO tool [15] developed by Oxford Nanopore Technologies (ONT), which is also integrated into the latest versions of Dorado as *dorado correct*. HERRO corrects erroneous R9.4 and R10.4 data, enabling their use as a replacement for accurate PacBio HiFi reads required by state-of-the-art hybrid assembly approaches. Supplementary Table S1 shows the estimated sequencing depth of coverage before and after the HERRO correction for each dataset.

For the high-coverage D2 *E.coli* dataset, Hifiasm outputs a fragmented assembly, while Verkko requires extensive parameter tuning (specifically in terms of coverage, `--unitig-abundance`, and `--base-k`) to achieve desirable contiguity and completeness. LJA produces an almost perfect assembly when a minimum length filter of 30kbp is applied to the corrected reads, as suggested by the HERRO paper. Flye performs comparably to LJA without the need for error correction.

For the other datasets, with or without error correction, most assemblers either fail to produce assemblies or generate suboptimal results, except for Flye. We attribute this to their sensitivity to inaccuracies in the uncorrected reads and the reduced coverage after correction. Supplementary Table S1 shows how the coverage levels change after correction for each dataset. Notably, Flye works well (and sometimes even slightly better) with uncorrected reads, highlighting its robustness to noisy ONT reads.

Based on these observations, we select Flye as the assembler to generate the gold standard assemblies in our evaluations, given its ability to handle noisy ONT reads without the need for error correction and its consistent performance across different datasets. Therefore, we use Flye to construct the gold standard assemblies from the basecalled reads in our study.

Table S1: Coverage levels before and after error correction for each dataset.

Dataset	Coverage Before Correction	Coverage After Correction
D2 <i>E. coli</i>	445×	240×
D3 <i>Yeast</i>	32×	12×
D4 <i>Green algae</i>	5.6×	3.7×
D5 <i>Human</i>	0.6×	0.002×

D. Configuration

D.1. Parameters

In Supplementary Table S2, we show the parameters of each tool for each dataset. In Supplementary Table S3, we show the details of the preset values that Rawsambl sets in Supplementary Table S2. For minimap2 [3], we use the same parameter setting for all datasets. For miniasm [4], we use the default parameter settings for all datasets.

Table S2: Parameters we use in our evaluation for each tool and dataset in mapping.

Tool	D1 SARS-CoV-2	D2 E. coli	D3 Yeast	D4 Green Algae	D5 Human
Rawsambl	-x ava-viral -t 32	-x ava -t 32	-x ava -t 32	-x ava -t 32	-x ava -chain-gap-scale 0.6 -t 32
Minimap2	-x ava-ont -for-only -t 32				
Dorado CPU (Fast)	basecaller -x cpu dna_r9.4.1_e8_fast@v3.4				
Dorado CPU (HAC)	basecaller -x cpu dna_r9.4.1_e8_hac@v3.3				
Dorado GPU (HAC)	basecaller dna_r9.4.1_e8_hac@v3.3				
Dorado GPU (SUP)	basecaller dna_r9.4.1_e8_sup@v3.3				
Miniasm					

Table S3: Corresponding parameters of presets (-x) in Rawsambl.

Preset	Corresponding parameters	Usage
ava-viral	-e 6 -q 4 -w 0 -sig-diff 0.45 -fine-range 0.4 -min-score 20 -min-score2 30 -min-anchors 5 -min-mapq 5 -bw 1000 -max-target-gap 2500 -max-query-gap 2500 -chain-gap-scale 1.2 -chain-skip-scale 0.3	Viral genomes
ava	-e 8 -q 4 -w 3 -sig-diff 0.45 -fine-range 0.4 -min-score 40 -min-score2 75 -min-anchors 5 -min-mapq 5 -bw 5000 -max-target-gap 2500 -max-query-gap 2500	Default case

D.2. Versions

Supplementary Table S4 shows the version and the link to these corresponding versions of each tool we use in our experiments.

Table S4: Versions of each tool and library.

Tool	Version	Link to the Source Code
Rawsambl	2.1	https://github.com/CMU-SAFARI/RawHash/releases/tag/v2.1
Minimap2	2.24	https://github.com/lh3/minimap2/releases/tag/v2.24
Dorado	0.7.3	https://github.com/nanoporetech/dorado/releases/tag/v0.7.3
Miniasm	0.3-r179	https://github.com/lh3/miniasm/releases/tag/v0.3
Rawasm	main	https://github.com/CMU-SAFARI/rawasm
Flye	2.9.5	https://github.com/mikolmogorov/Flye/releases/tag/2.9.5
HERRO	0.1	https://github.com/lbcb-sci/herro

Supplementary References

- [1] C. Firtina *et al.*, "RawHash: enabling fast and accurate real-time analysis of raw nanopore signals for large genomes," *Bioinform.*, 2023.
- [2] C. Firtina *et al.*, "RawHash2: Mapping Raw Nanopore Signals Using Hash-Based Seeding and Adaptive Quantization," *Bioinform.*, 2024.
- [3] H. Li, "Minimap2: pairwise alignment for nucleotide sequences," *Bioinform.*, 2018.
- [4] H. Li, "Minimap and miniasm: fast mapping and de novo assembly for noisy long sequences," *Bioinform.*, 2016.
- [5] R. R. Wick *et al.*, "Bandage: interactive visualization of de novo genome assemblies," *Bioinform.*, 2015.
- [6] J. Sun *et al.*, "Benchmarking oxford nanopore read assemblers for high-quality molluscan genomes," *Philosophical Transactions of the Royal Society*, Apr. 2021.
- [7] R. R. Wick and K. E. Holt, "Benchmarking of long-read assemblers for prokaryote whole genome sequencing," *F1000Research*, 2021.
- [8] B.-M. Cosma *et al.*, "Evaluating long-read de novo assembly tools for eukaryotic genomes: insights and considerations," *GigaScience*, 2022.
- [9] W. Yu *et al.*, "Comprehensive assessment of 11 de novo hifi assemblers on complex eukaryotic genomes and metagenomes," *Genome Research*, 2024.
- [10] H. Cheng *et al.*, "Haplotype-resolved de novo assembly using phased assembly graphs with hifiasm," *Nature Methods*, 2021.
- [11] M. Rautiainen *et al.*, "Telomere-to-telomere assembly of diploid chromosomes with verkko," *Nature Biotechnology*, 2023.
- [12] A. Bankevich *et al.*, "Multiplex de bruijn graphs enable genome assembly from long, high-fidelity reads," *Nature Biotechnology*, 2022.
- [13] S. Nurk *et al.*, "Hicanu: accurate assembly of segmental duplications, satellites, and allelic variants from high-fidelity long reads," *Genome Research*, 2020.
- [14] M. Kolmogorov *et al.*, "Assembly of long, error-prone reads using repeat graphs," *Nature Biotechnology*, 2019.
- [15] D. Stanojevic *et al.*, "Telomere-to-telomere phased genome assembly using error-corrected simplex nanopore reads," *arXiv*, 2024.